Proceeding of the IEEE
International Conference on Robotics and Biomimetics
Dali, China, December 2019

A Novel Obstacle Collision Avoidance Strategy for Redundant Manipulator using Swivel Motion Control

Kunlin Guo
College of Automation Science and Engineering
South China University of Technology
Guangzhou, Guangdong Province, China

Yiming Jiang
College of Electrical and Information Engineering
Hunan University
Changsha, Hunan Province, China

Xinyu Wu
Shenzhen Institutes of Advanced Technology
Chinese Academy of Sciences
Shenzhen, Guangdong Province, China

Chenguang Yang
Bristol Robotics Laboratory
University of the West of England
Bristol, BS16 1QY, UK

***Abstract*— The research of humanoid 7-DoF redundant robotic manipulator has attracted increasing attention, due to its importance of using the redundancy to accomplish sub-tasks. In this paper, a novel obstacle collision avoidance strategy is proposed for the redundant manipulator. At first, a controller of swivel angle defined by a plane consists of the robot's shoulder, elbow and wrist joints is designed. Then, a null space based controller is developed to avoid a moving obstacle by controlling the swivel angle's motion. The designed swivel motion controller is not only to guarantee the end-effector tacking the desired trajectory precisely but also to accomplish obstacle avoidance task in the sub-space with the virtual repulsive force pushing from the obstacle to the swivel joints. The feasibility of the proposed control strategy is proved by simulation experiments based on a 7-DoF redundant robot.**

***Index Terms*— redundant manipulator, null-space, swivel control, obstacle avoidance**

I. Introduction

In recent years, research on redundant manipulators has attracted more and more attention due to the advantages brought by its redundancy and flexibility, and many achievements have been made in different applications such as obstacle avoidance, impedance control, and human-robot interaction. The most important characteristic of a redundant manipulator is the abundant of joints degree, which enables the manipulator to accomplish tasks that non-redundant robotic manipulator cannot, such as, avoiding singular configuration, avoiding joint limit, approaching the target point with different posture.

Redundant manipulator is known as a robotic manipulator with n degree of freedom (DoF) operating in the task space of m dimensional Cartesian space, satisfying $n > m$. Since the complexity of its structure, the control of a redundant manipulator is always more difficult than a non-redundant robotic manipulator, especially when calculating the inverse kinematics. In [1], researchers used the gradient method to calculate the inverse kinematics basing on the real-time planned path, then the priorities of the distance between manipulator and obstacles and the priorities of the singular position was considered as the fixing joint angles strategy was introduced. Later, a novel redundant manipulator control strategy was proposed in [2], which incorporated the redundancy into the controller to accomplish a sub-task. It was shown that the controller was suitable for the containment control of the redundant manipulator.

A novel redundant manipulator control strategy is the null-space control strategy, [3] shows that by dividing manipulator controller into task-space controller and null-space controller, the manipulator can complete the main-task and the sub-task at the same time. Through adding priority division, the error of the main-task such as trajectory tracking can be reduced to a very small value, while the sub-task such as avoiding singular configuration or avoiding joint limit can have a good performance. Also, the null-space control strategy has good stability performance under external disturbance [4].

A special null-space control strategy has been proposed for a 7-DoF humanoid redundant manipulator known as the swivel controller [5]- [8]. As the structure of human arm, the shoulder, elbow and wrist joints of a 7-DoF redundant manipulator, which could be regarded as a whole plane to control which can also be treated as the one redundant DoF. This theory has already achieved many results, such as guaranteeing the posture during a surgical task [5], [6], imitating human performance basing on artificial neural network [7], improving the synergistic relationship between the exoskeleton and the operator [8].

For obstacle avoidance problem, one of the most commonly used methods is the artificial potential field method, whose core is to construct the repulsive force field around the

This work was partially supported by Engineering and Physical Sciences Research Council (EPSRC) under Grant EP/S001913. Corresponding author is C. Yang. Email: cyang@ieee.org.

978-1-7281-6321-5/19//$31.00 ©2019 IEEE

obstacle and the attractive force field to avoid the collision between the mechanical arm and the obstacle as well as pulling the end-effector toward the target point effectively [9], [10].

As for redundant manipulators, the task of avoiding obstacle have more solution because of the redundancy. In [11], the traditional artificial potential field method was improved by introducing the repulsion field to the two points on the obstacle with the shortest distance to the manipulator joint, which could avoid the obstacle successfully however would take too much calculation. A minimum distance indicator using the RRT algorithm and null-space matrix was proposed in [12] for 7-DOF YuMi redundant manipulator's obstacle avoidance problem, whose obstacle avoidance strategy has better efficiency.

In this paper, inspired by the swivel motion control, we proposed a control framework for robot Baxter's left arm, a 7-DoF redundant manipulator, which enables obstacle avoidance of the robot by embedding the null space based swivel angle control into the controller design. Additionally, a force field is designed such that a virtual repulsive force is added to the swivel angle in terms of the distance between the obstacle and the robot.

The rest of this paper is organized as follows. Preliminaries of the redundant robots and null-space control strategy are given in Section II. The swivel motion control strategy and the optimized artificial potential field method are given in Section III. Simulation results are presented in Section IV to testify the proposed swivel motion controller with external force disturbance and obstacle avoidance respectively. Finally, conclusions are given in Section V.

II. PRELIMINARIES

A. System Description of Redundant Robots

In this paper we studied the redundant robotic manipulator with n DoF operating in the m dimensional Cartesian space while $m < n$. The dynamic model written in Lagrangian form represented as follows:

$$M(q)\ddot{q} + D(q,\dot{q}) + g(q) = \tau_c - \tau_e \tag{1}$$

where vector $q \in R^n$ and matrix $M(q) \in R^{n\times n}$ respectively denote the joint angle vector and the inertia matrix, Coriolis and Centrifugal effects is represented by matrix $D(q,\dot{q}) \in R^{n\times n}$ and vector $g(q) \in R^n$ is denoting the gravity torques. The two torque terms $\tau_c \in R^n$ and $\tau_e \in R^n$ are respectively representing the control torque applied on manipulators of robot and the external torque vector applied on the manipulator. Therefore, the controller of the manipulator system can be designed as follows:

$$\tau_c = \tau_d + \hat{D}(q,\dot{q})\dot{q} + \hat{g}(q) + \hat{\tau}_e \tag{2}$$

where matrix $\hat{D}(q,\dot{q}) \in R^{n\times n}$ and vector $\hat{g}(q)$ are the estimated compensation of Coriolis term and gravity torque term respectively, vector $\hat{\tau}_e$ is the external torque after filtered computed through the external torque sensors and vector τ_d is the controller torque applying on the manipulator to accomplish the desired end-effector control performance, which is defined as follows:

$$\tau_d = \tau_t + \tau_n \tag{3}$$

where the first control torque represented by $\tau_t \in R^n$ is the control torque ensuring the implementation of the main task, i.e. the end-effector position tracking. Simultaneously, the second control torque represented by $\tau_n \in R^n$ is the sub-task control torque, implementing additional tasks in the null-space in addition to the main task.

B. Task-Space Control Strategy

To reach the goal of tracking the desired end-effector trajectory X_d precisely, after considering existing manipulator control strategies comprehensively, the compliance control strategy is designed. By using the energy function of the potential spring system definition and adding damping energy term as used in [13], we design the main task control torque as follows:

$$\tau_t = J^T F_T = J^T \left(\left(\frac{\partial P(X_e)}{\partial X} \right)^T - D_x \dot{X} \right) \tag{4}$$

where the positive definite diagonal matrix $D_x \in R^{m\times m}$ is the consistent damping parameter matrix. For further explanation, the function $P(X_e)$ is defined as the virtual spring potential system as follows:

$$P(X_e(q)) = \frac{1}{2} X_e(q)^T K_x X_e(q) \tag{5}$$

where the positive definite diagonal matrix $K_x \in R^{m\times m}$ is the consistent stiffness parameter as defined in the compliance law. The difference between the desired tracking trajectory and the actual trajectory of the end-effector in the Cartesian space is represented by the function X_e, which is defined by the desired end-effector trajectory X_d and actual cartesian position X as follows:

$$X_e(q) = X_d - X(q) \tag{6}$$

In the following section, a null-space control strategy is proposed to deal with the problem of interacting with the manipulator's body physically during the process of accomplishing the main task.

C. Null-Space Control Strategy

As defined in (2) and (3), the control torque τ_d is divided into τ_t and τ_n respectively, providing the ability of accomplishing sub-task in addition to the main task conducted by main task torque τ_t as sub-task torque τ_n. To ensure that the primary task $\tau_t$takes precedence over the secondary task, strict hierarchical projections is applied where high-priority

tasks are decoupled from low-priority tasks. This implies that low-priority tasks would be conducted as well as possible as long as the performance of high-priority tasks is not affected. Therefore, the sub-task conducted in null-space can be defined as:

$$\tau_n = N \cdot \tau_s = \left[I - J(q)^T \left(J(q)^\sharp \right)^T \right] \tau_s \tag{7}$$

where $N \in R^{n\times n}$ represents the null-space matrix and $J(q)^\sharp \in R^{n\times n}$ is the weighted generalized inverse denoted by $J(q)^\sharp = U^{-1}J^T\left(JU^{-1}J^T\right)^{-1}$, while $U \in R^{n\times n}$ is a symmetric positice definite matrix. The control torque $\tau_s \in R^{n\times n}$ represents a secondary task. In order to guarantee a dynamic consistency of the system, that there is no interference between the hierarchic levels in the transient and steady state, the generalized weighted inverse is calculated through: $U = M(q)$, resulting in the inertia-weighted pseudo-inverse $J(q)^\sharp \in R^{n\times m}$ [14].

In order to accomplish both the main task and the sub-task of the robot at the same time under guaranteeing the main task is the high-priority task, the null-space of the redundant manipulator can be used to complete the low-priority tasks while maintaining the physical contract between the main task and the robot body.

III. Controller Design for 7-DoF Redundant Manipulator

In this paper, our research object is the left arm of Baxter robot, the humanoid 7-DoF ($n = 7$) redundant manipulator as shown in Fig. 1. Since the working space is the six dimensions Cartesian space as $m = 6$, the number of redundancy in this paper is: $r = n - m = 7 - 6 = 1$.

A. Swivel Motion Controller Design

As shown in Fig. 1, we define the angle between the swivel plane and the basic plane as the swivel angle ψ. According to Fig. 1, $\psi \in R$ is measured around the axis $\overrightarrow{BD}$, pointing from the manipulator arm's shoulder joint to the wrist joint. Making use of geometric relations, the swivel angle is calculated as follows:

$$\begin{aligned}\psi = & sign\left(\left(\overrightarrow{AB}\times\overrightarrow{BC}\right)\cdot\overrightarrow{BD}\right)\times \\ & cos^{-1}\left(\frac{\left(\overrightarrow{AB}\times\overrightarrow{BD}\right)\cdot\left(\overrightarrow{BC}\times\overrightarrow{CD}\right)}{\|\overrightarrow{AB}\times\overrightarrow{BD}\|\cdot\|\overrightarrow{BC}\times\overrightarrow{CD}\|}\right)\end{aligned} \tag{8}$$

where $\overrightarrow{AB}$ is the vector pointing from the manipulator arm's base to the shoulder joint, $\overrightarrow{BC}$ is the vector pointing from the manipulator arm's shoulder joint to the elbow joint, $\overrightarrow{BD}$ is the vector pointing from the manipulator arm's shoulder joint to the wrist joint and $\overrightarrow{CD}$ is the vector pointing from the manipulator arm's elbow joint to the wrist joint.

Unlike other studies discussing null space compliance control through joint space, the compliance control strategy

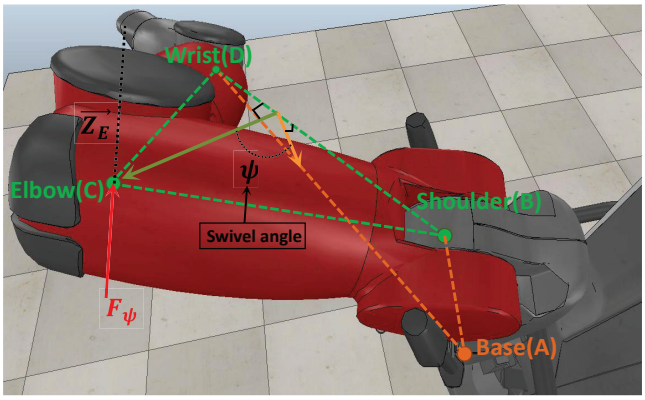

Fig. 1. Definition of swivel angle ψ and the virtual control force F_ψ.

of null space is accomplished through swivel motion control in our study. This solution enables the robot arm's swivel angle ψ maintaining its initial angle ψ_{ini} with a compliant control strategy. To realize the compliance control strategy, a virtual force $F_\psi \in R^{3\times 1}$ applying directly on the robots elbow joint along its joint axis $\overrightarrow{Z_E}$ is designed to control the robot arm's swivel motion effectively, which enables the robot arm system behave like a damper-spring system. Therefore, we can calculate the secondary task control torque τ_s proposed in Eq. (7) as follows:

$$\tau_s = \begin{bmatrix} 0 & \left(J_e^T F_\psi\right)^T & 0 & 0 \end{bmatrix}^T - \hat{\tau}_e \tag{9}$$

where J_e is the Jacobian matrix of part of the robot from the base to the elbow joint and it should be noticed that since the virtual force F_ψ only effect on the robot arm's swivel motion, other parts especially the first term of the secondary task control torque τ_s must be set as 0. Then the virtual force F_ψ is defined as follows:

$$\begin{aligned} F_\psi &= [0 \quad 0 \quad f_\psi], \\ f_\psi &= K_\psi(\psi_{ini} - \psi) - D_\psi\dot{\psi} \end{aligned} \tag{10}$$

where $K_\psi \in R$ and $D_\psi \in R$ are positive stiffness constant and positive damping constant respectively. Unlike other proposed controller, f_ψ was designed with the upper and lower bounds of ψ, the swivel motion controller proposed in this paper would not have the problem that mutations occur when ψ cross the boundaries [5].

As shown in (2), through the measured external torque $\hat{\tau}_e$ the external torque is compensated, which means that the main control task of the robot arm would not be disturbed by the external torque applied to the robot arm. It should be highlighted that though in most work the effect of external torque is considered in the main task, the null space motion in this work is driven by the external torque. Therefore, the measured external torque $\hat{\tau}_e$ is included in the secondary task control torque of the null space motion.

B. Potential Field

Potential field method is one of the most generally used methods for obstacle avoidance task in manipulator control. However, the pure potential field method using in obstacle avoidance tasks may cause too much calculation for robot joint planning. Therefore we to combine the potential field method with the swivel motion control strategy, investigating a new obstacle avoidance strategy with more efficiency, as shown in Fig. 2.

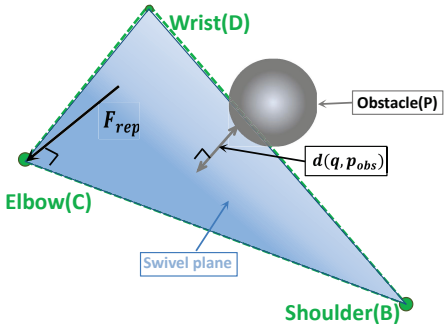

Fig. 2. Schematic diagram of swivel panle obstacle avodance strategy using potential field.

Since our main task is to track the desired end-effector trajectory precisely, the task of avoiding the obstacle is accomplished by the null-space through the swivel motion control. Therefore we only add the repulsive potential field without the attractive potential field compared to the general potential field method. In this way, we avoid the local minimum point problem. This is also one of the advantages of using null-space to realize the task of avoiding obstacle.

One of the commonly used repulsive potential field function takes the form as follows:

$$U_{rep}(q) = \begin{cases} \frac{1}{2}\eta\left(\frac{1}{d(q,p_{obs})} - \frac{1}{d_0}\right)^2, & \text{if } d(q, q_{obs}) \le d_0 \\ 0, & \text{if } d(q, p_{obs}) > d_0. \end{cases} \tag{11}$$

where η is the positive scaling factor, $p_{obs} \in R^{3\times 1}$ is the coordinate of the obstacle point, the positive constant d_0 representing the influence distance of the obstacle, and $d(q, q_{obs})$ represents the distance from the position of obstacle p_{obs} to the swivel plane q defined by robot arm's shoulder, elbow and wrist joints, that is, vectors $\overrightarrow{BC}$ and $\overrightarrow{CD}$, defined as follows:

$$d(q, p_{obs}) = \|\overrightarrow{CP}\| \cdot cos^{-1}\left(\frac{\left(\overrightarrow{AB} \times \overrightarrow{BC}\right) \cdot \overrightarrow{CP}}{\|\overrightarrow{AB} \times \overrightarrow{BC}\| \cdot \|\overrightarrow{CP}\|}\right) \tag{12}$$

where vector $\overrightarrow{CP}$ is pointing from the manipulator arm's elbow joint to the obstacle point. Then we can get the corresponding repulsive force through calculating the negative gradient of the repulsive potential function using ∇ as the gradient calculation symbol:

$$\begin{aligned} F_{rep}(q) &= -\nabla U_{rep}(q) \\ &= \begin{cases} \eta\left(\frac{1}{d(q,p_{obs})} - \frac{1}{d_0}\right)\nabla d(q, p_{obs}), & \text{if } d(q, p_{obs}) \le d_0 \\ 0, & \text{if } d(q, p_{obs}) > d_0 \end{cases} \end{aligned} \tag{13}$$

IV. EXPERIMENT RESULTS

In this section, we show the simulation experiment results obtained by adopting the robot motion control strategy proposed in Section III. The simulation experiment is conducted based on Matlab and Simulink, while the simulation manipulator is the left arm of the Baxter robot. In the first experiment, the feasibility of the proposed swivel motion controller is verified. Without the swivel motion controller, once the external force is applied to the manipulator, the manipulator arm's posture would be changed, therefore the end-effector would be affected, being unable to track the desired trajectory precisely. In the second experiment, there is an obstacle object moving towards the manipulator. By introducing the artificial potential field method, the improved swivel motion controller proposed in this paper can succeed in avoiding the collision between the manipulator and the obstacle without affecting the desired trajectory tracking task.

The block flamework of the whole control system is shown in Fig. 3. It is clear that both the external disturbance and obstacle avoidance are solved through the null space controller in the inner loop, which would have no impact on the main task.

It should be highlighted that according to [15], when a robotic system perfroming a task, maintaining the elbow down posture can help it reduce the energy consumption. Therefore, the initial joint angles of the robot in our experiment are set as $q_0 = [0\ 0.7854\ 0\ \ -1.5708\ 0\ 0.7854\ 0]$ to maintain the elbow down posture as shown in Fig.4, and the initial swivel angle ψ_{ini} is 0. Furthermore, the compliance parameters are set to $K_x = diag([600\ 600\ 600\ 1\ 1\ 1])$N/m, $D_x = diag([50\ 50\ 50\ 0\ 0\ 0])$Ns/m, $k_\psi = 30$N/rad and $d_\psi = 0.5$rad/s. The desired trajectory for end-effector tracking as the main task is designed as: $X_d = 0.7791 + 0.02 \times t$ m.

A. First Experiment: Swivel Motion Control

In this experiment, we verified that when the manipulator is disturbed by external force in the process of end-effector main task of tracking the desired trajectory X_d. The proposed swivel motion controller can ensure the end-effector to track the desired trajectory precisely.

The external force F_e applied on the manipulator along the y axis is designed as: $F_e = 0.5 \times sin(t \times \frac{\pi}{10}) + 0.5$ N which is shown in Fig. 5. The tracking error of the end-effector and the swivel angle ψ without the external force applied on the manipulator are respectively shown in Fig. 6 and Fig.7.

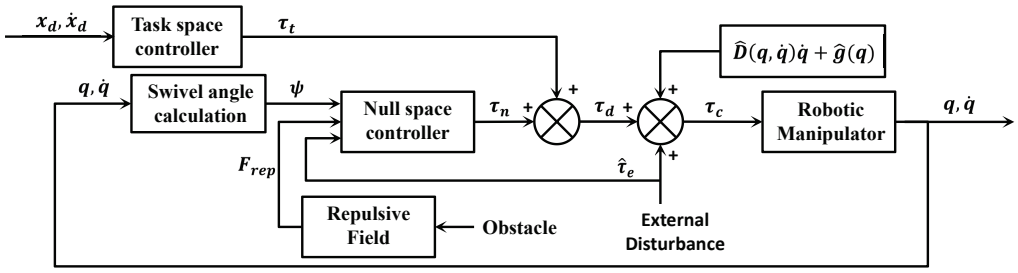

Fig. 3. Block framework of the whole control system

Fig. 8 and Fig. 9 show the tracking error of end-effector and the swivel angle ψ respectively when the external force is applied on the manipulator.

According to Fig. 6 and Fig. 8 we can draw the conclusion that the main task of end-effector trajectory tracking can be accomplished precisely either with or without external force disturbance. Also, the swivel motion control strategy is activated effectively to reduce the impact of the external force applied on the manipulator arm as shown in Fig. 7 and Fig.9.

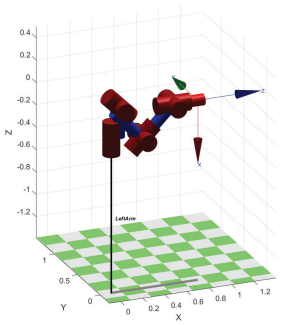

Fig. 4. The simulation model of left arm of Baxter robot.

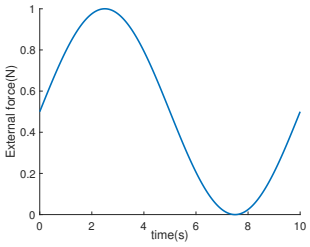

Fig. 5. External force F_e applied on the manipulator in first experiment.

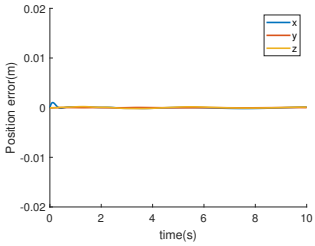

Fig. 6. Position error X_e of first experiment without external force.

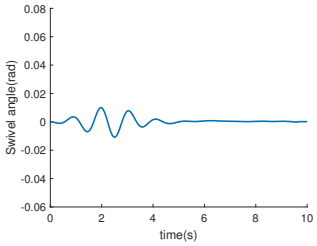

Fig. 7. Swivel angle ψ of first experiment without external force.

B. Second Experiment: Obstacle Avoidance

In this experiment, a moving obstacle is inducted following the trajectory: $p_{obs} = -0.05 \times t + 0.45$, with the influence distance $d_0 = 0.2$m and $\eta = 1$, which can be regarded as a

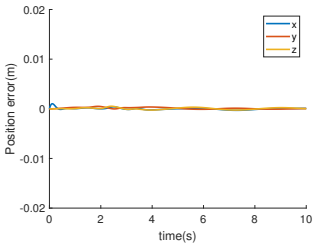

Fig. 8. Position error X_e of first experiment with external force.

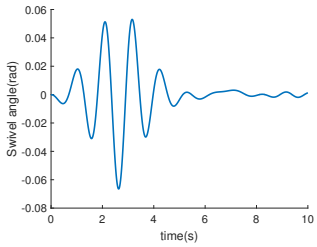

Fig. 9. Swivel angle ψ of first experiment with external force.

moving elastic ball of radius 0.2m as shown in Fig. 14. To accomplish the secondary task of avoiding the collision of manipulator arm and the obstacle without affecting the end-effector trajectory tracking task, the potential field method introduced in Section III is combined with the swivel motion control strategy, therefore the virtual force F_ψ is updated as follows:

$$F_\psi^o = F_\psi + F_{rep} = [0 \quad 0 \quad f_\psi + F_{rep}] \tag{14}$$

The experiment results are shown in figures from Fig.10 to Fig.12.

The distances of obstacle to the manipulator arm with and without the potential field method are shown in Fig. 10 respectively as blue line and red dot line. It can be seen that once without the repulsive force, the distance in Fig. 10 reaches 0, meaning that the collision between the manipulator and the obstacle would happen if there doesn't have any avoiding strategy, as shown in Fig. 15 that the red dot obstacle is contacting with the manipulator. In Fig. 14 we can see the swivel motion controller is working to avoid the red dot obstacle. The distance in Fig. 10 is always larger than 0 since the potential field method is activated as the repulsive force shown in Fig. 11. The repulsive force shown in Fig. 11 remains 0 before 5s for the reason that the distance of the obstacle is larger than $d_0 = 0.2$. In this case, the tracking error of the end-effector is shown in Fig. 13, which indicates that there is no significant impact on the end-effector tracking task. The swivel angle ψ over time is shown in Fig. 12, where we can see that the swivel motion control strategy helps the manipulator arm effectively avoid the collision of the obstacle

by changing the swivel angle ψ to change the posture of the manipulator as shown in Fig. 14.

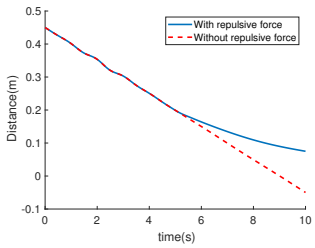

Fig. 10. Distance of obstacle to manipulator with and without repulsive force.

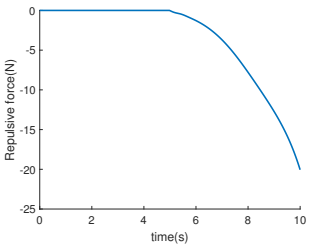

Fig. 11. Repulsive force F_{rep} generate by the distance of obstacle to manipulator.

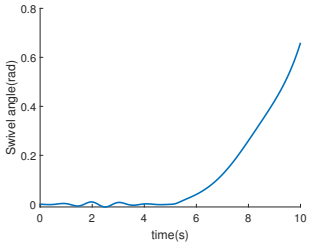

Fig. 12. Swivel angle ψ of the second experiment.

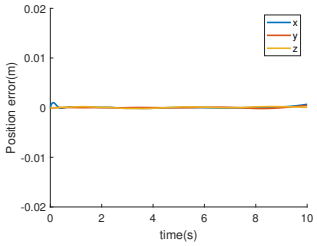

Fig. 13. Tracking error X_e of the second experiment.

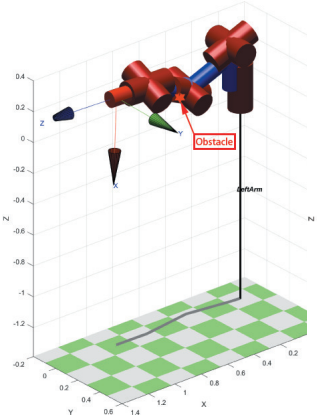

Fig. 14. Manipulator posture with repulsive force and the red dot of obstacle at t=8s.

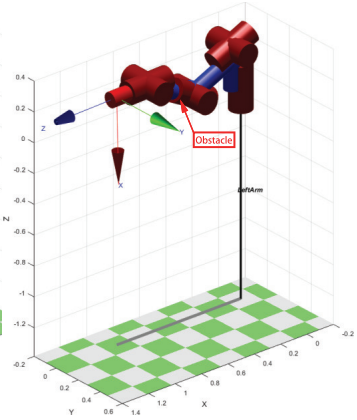

Fig. 15. Manipulator posture without repulsive force and the red dot of obstacle at t=8s.

V. CONCLUSION

In this paper, we propose a novel swivel motion control framework for the 7-DoF redundant manipulator, considering a plane of the swivel motion composed by the shoulder, elbow and wrist joints of the robot, a null based controller is constructed to control the swivel motion, which could resist the interference of external force effectively as proved in the experiment results. Moreover, in order to make full use of the swivel motion controller and the redundancy of the 7-DoF manipulator, we transformed the artificial potential method into the repulsive field method to enable the swivel motion to avoid the obstacle. Experiment results on a 7-DoF Baxter robot show the feasibility of the proposed controllers.

REFERENCES

[1] H. Zhang, H. Jin, Y. Liu and H. Yuan, "An improved real-time tracking scheme based on gradient projection for kinematically redundant manipulators," 2017 2nd International Conference on Robotics and Automation Engineering (ICRAE), Shanghai, 2017, pp. 136-140.

[2] A. Zakerimanesh, A. Torabi, F. Hashemzadeh and M. Tavakoli, "Task-Space Position and Containment Control of Redundant Manipulators with Bounded Inputs," 2019 IEEE 15th International Conference on Automation Science and Engineering (CASE), Vancouver, BC, Canada, 2019, pp. 431-436.

[3] T. Makinouchi and T. Murakami, "High performance force control for cooperative of null space and task space motion in redundant manipulator," 9th IEEE International Workshop on Advanced Motion Control, 2006., Istanbul, 2006, pp. 177-182.

[4] Y. Ping, S. Hanxu and J. Qingxuan, "Study on Kinematics Optimization of Redundant Manipulators," 2006 IEEE Conference on Robotics, Automation and Mechatronics, Bangkok, 2006, pp. 1-6.

[5] J. Sandoval, H. Su, P. Vieyres, G. Poisson, G. Ferrigno, E. De Momi, "Collaborative framework for robot-assisted minimally invasive surgery using a 7-DoF anthropomorphic robot", in Robotics and Autonomous Systems, vol. 106, pp. 95-106, 2018.

[6] H. Su, S. Li, J. Manivannan, L. Bascetta, G. Ferrigno and E. D. Momi, "Manipulability Optimization Control of a Serial Redundant Robot for Robot-assisted Minimally Invasive Surgery," 2019 International Conference on Robotics and Automation (ICRA), Montreal, QC, Canada, 2019, pp. 1323-1328.

[7] H. Su, W. Qi, C. Yang, A. Aliverti, G. Ferrigno and E. De Momi, "Deep Neural Network Approach in Human-Like Redundancy Optimization for Anthropomorphic Manipulators," in IEEE Access, vol. 7, pp. 124207-124216, 2019.

[8] H. Kim, J. R. Roldan, Z. Li and J. Rosen, "Viscoelastic model for redundancy resolution of the human arm via the swivel angle: Applications for upper limb exoskeleton control," 2012 Annual International Conference of the IEEE Engineering in Medicine and Biology Society, San Diego, CA, 2012, pp. 6471-6474.

[9] W. Guan, Z. Weng and J. Zhang, "Obstacle avoidance path planning for manipulator based on variable-step artificial potential method," The 27th Chinese Control and Decision Conference (2015 CCDC), Qingdao, 2015, pp. 4325-4329.

[10] N. Zhang, Y. Zhang, C. Ma and B. Wang, "Path planning of six-DOF serial robots based on improved artificial potential field method," 2017 IEEE International Conference on Robotics and Biomimetics (ROBIO), Macau, 2017, pp. 617-621.

[11] W. Wang, J. Gu, M. Zhu, Q. Huo, S. He and Z. Xu, "An obstacle avoidance method for redundant manipulators based on artificial potential field," 2018 IEEE International Conference on Mechatronics and Automation (ICMA), Changchun, 2018, pp. 2151-2156.

[12] Z. Xu, Y. Gan and X. Dai, "Obstacle avoidance of 7-DOF Redundant Manipulators," 2019 Chinese Control And Decision Conference (CCDC), Nanchang, China, 2019, pp. 4184-4189.

[13] A. Dietrich, T. Wimbock, A. Albu-Schaffer and G. Hirzinger, "Integration of Reactive, Torque-Based Self-Collision Avoidance Into a Task Hierarchy," in IEEE Transactions on Robotics, vol. 28, no. 6, pp. 1278-1293, Dec. 2012.

[14] O. Khatib, "A unified approach for motion and force control of robot manipulators: The operational space formulation," in IEEE Journal on Robotics and Automation, vol. 3, no. 1, pp. 43-53, February 1987.

[15] P. Khalaf and H. Richter, "Trajectory Optimization of Robots With Regenerative Drive Systems: Numerical and Experimental Results," in IEEE Transactions on Robotics.